

Rayleigh-Bénard thermal convection perturbed by a horizontal heat flux

Jinzi Mac Huang^{1,2†} and Jun Zhang^{1,2,3‡}

¹NYU-ECNU Institute of Physics and Institute of Mathematical Sciences, New York University Shanghai, Shanghai, China

²Applied Math Lab, Courant Institute, New York University, New York, USA

³Department of Physics, New York University, New York, USA

(Received xx; revised xx; accepted xx)

In Rayleigh-Bénard convection, it has been found that the amount of heat passing through the fluid has a power law dependence on the imposed temperature difference. Modifying this dependence, either enhancing or reducing the heat transfer capability of fluids, is important in many scientific and practical applications. Here, we present a simple means to control the vertical heat transfer in Rayleigh-Bénard convection by injecting heat through one lateral side of the fluid domain and extracting the same amount of heat from the opposite side. This horizontal heat flux regulates the large-scale circulation, and increases the heat transfer rate in the vertical direction. Our numerical and theoretical studies demonstrate how a classical Rayleigh-Bénard convection responds to such a perturbation, when the system is near or well above the onset of convection.

1. Introduction

There are many similarities between thermal, electronic, and fluid systems. For example, Ohm's law relates a flux of charges to an electrostatic potential difference, while Fourier's law of heat conduction $|q| \propto \Delta T$ states that heat flux $|q|$ is proportional to the temperature difference ΔT . Other physical laws also share similar mathematical forms, such as the conservation laws (Evans 2010) regarding electrical charge, energy, and mass. Drawing analogies between these different systems has revealed many mechanisms that are known in one system but less obvious in the other (Schönfeld 1954). Examples include the fluid "transistor" circuits proposed more than 60 years ago (Pursglove 1960) and a recent example on the flow rectifier based on Nikola Tesla's concept of a fluidic diode (Nguyen *et al.* 2021a,b).

Combining these systems also reveals nontrivial and sometimes surprising dynamics. For example, allowing mass flow to a thermal system introduces nonlinearity that Fourier's law does not capture. It is well known that thermal convection appears when temperature gradient exceeds a threshold (Busse 1978; Niemela *et al.* 2000; Childress 2009). One canonical example is the Rayleigh-Bénard convection (RBC), whose configuration is simple: a closed domain of fluid is subject to heating from the bottom and cooling from the top, while the sidewalls remain adiabatic, as shown in Fig. 1(a). The cooled fluid near the top plate is heavier than the heated fluid near the bottom, creating an instability under gravity. Convection occurs when this system is beyond a threshold or onset, and the vertical heat flux has been observed to depend on the temperature difference nonlinearly: $|q| \propto \Delta T^\gamma$ where γ is around 1.3, for a wide range of external and fluid parameters (Belmonte *et al.* 1994; Grossmann & Lohse 2000; Ahlers *et al.* 2009).

There have been numerous attempts to modify the heat transport in RBC and deviate from the

† Email address for correspondence: machuang@nyu.edu

‡ Email address for correspondence: jz11@nyu.edu

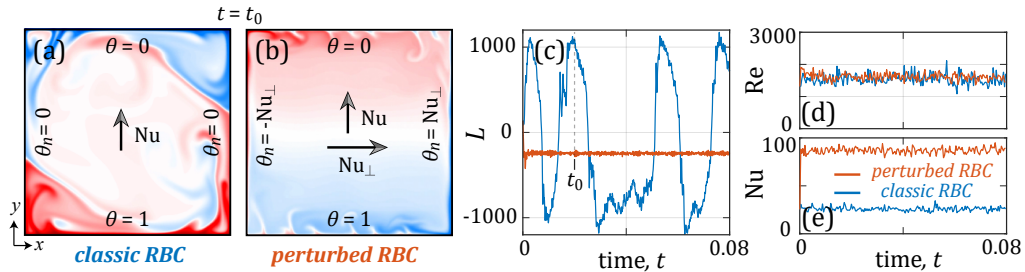


FIGURE 1. At $Ra = 10^8$ and $Pr = 4.4$, flow and thermal structures of (a) A classic RBC; (b) A perturbed RBC, where a horizontal heat flux is added through sidewall flux conditions. (c) In classic RBC, the total angular momentum $L(t)$ (blue data) alternates between positive and negative values due to the reversals of the large-scale circulation. In the perturbed case (red data), $L(t)$ stays negative and stable as the large-scale circulation is always clockwise (CW). (d) Defined by the maximum flow velocity (Section 2), the Reynolds number of both the classic and perturbed RBC is similar. (e) The Nusselt number is significantly enhanced by introducing the horizontal flux. The horizontal flux in (b)-(e) is $Nu_{\perp} = 128$. The time $t = t_0$ of snapshots (a) and (b) is marked in (c), and full videos of (a) and (b) are included in the Supplements.

above dependency, as a reduced or enhanced heat transfer rate is sometimes desired in applications like effective ventilation or energy preservation. Successful experimental examples include adding rotation to the RBC (Stevens *et al.* 2009; Zhong & Ahlers 2010), where moderate rotation rates enhance the heat flux and high rates reduces heat flux; changing the surface roughness of the top and bottom plates (Du & Tong 1998), where corrugated surface patterns result in higher heat transfer. Tilting the convection cell (Wang *et al.* 2018; Guo *et al.* 2015) or inserting insulating partitions into the fluid domain (Bao *et al.* 2015) also leads to regulated circulation and higher overall heat transfer rate. Combined experimental and numerical efforts have also brought insights on heat transport enhancement through coherent structure manipulation (Chong *et al.* 2017).

The examples above show the possibility of modifying the heat transfer in Rayleigh-Bénard convection, and many of them involve adding mechanical parts or changing the geometry of the convection cell. Without moving parts, an active control of Rayleigh-Bénard convection through modified boundary conditions is also possible. Examples include the work of Howle (1997), where the unstable convective fluid motion is stabilized through an active heat flux imposed through the boundary conditions, and the study by Zhang *et al.* (2020), where the reversal of large-scale circulation is suppressed by introducing small control regions on the sidewalls.

In order to externally control and enhance the heat transfer, we impose a horizontal heat flux q_{\perp} to the classical Rayleigh-Bénard convection as shown in Fig. 1(b), by setting sidewall temperature gradients as $|\partial_n T| = q_{\perp}/K$, where K is the thermal conductivity. This additional flux, by heating on one side and cooling on the opposite side, modifies the bulk fluid motion by inducing buoyancy jets near the sidewalls, resulting in a unidirectional large-scale circulation as seen in Fig. 1(b), where the fluid angular momentum L (defined in Section 2) ceases to alternate as shown in Fig. 1(c). Interestingly, the overall magnitude of flow angular momentum is reduced while the flow velocity, measured by the Reynolds number (Section 2), stays nearly unchanged in Fig. 1(c)-(d). On the other hand, the vertical heat transfer rate measured by the Nusselt number (Section 2) in Fig. 1(e) is greatly increased compared to the classic case.

To understand these observations, we examine the side-heated and side-cooled Rayleigh-Bénard convection systematically through two-dimensional (2D) numerical simulations. Considering that the flow and thermal structures involved are largely 2D, especially when side heating and cooling dictate the flows, the heat transfer properties of Rayleigh-Bénard convection can be accurately accounted for by such numerical simulations (Schmalzl *et al.* 2002, 2004; Ahlers *et al.* 2009).

2. Numerical setup

To formulate our problem dimensionlessly, we rescale temperature T by $\Delta T = T_b - T_t$ so the dimensionless temperature is $\theta = (T - T_t)/\Delta T$, and rescale coordinates (X, Y) by L (domain height) so the coordinates $(x, y) \in \Omega \triangleq (0, 1) \times (0, 1)$, as shown in Fig. 1(a). The time is rescaled by the thermal diffusion time scale of L^2/κ where κ is the thermal diffusivity of the fluid, leading to the dimensionless velocity field $\mathbf{u} = UL/\kappa$. Two relevant dimensionless numbers are the Rayleigh number $\text{Ra} = \alpha g \Delta T L^3 / \kappa \nu$, which measures the relative strength between the thermally induced buoyancy force and the fluid viscous force, and the Prandtl number $\text{Pr} = \nu / \kappa$, the ratio between fluid viscosity and thermal diffusivity. Here ρ, ν, α and g are the density, kinematic viscosity, and thermal expansion coefficient of the fluid and the acceleration due to gravity, respectively.

The heat flux passing through the vertical direction can be non-dimensionalized as the Nusselt number, $\text{Nu} = q/q_c = -\int_0^1 \partial_y \theta(x, 1) dx$, which is the ratio between the convective flux $q = -(K/L) \int_0^L \partial_Y T(X, L) dX$ and the conductive flux $q_c = K \Delta T / L$. To simplify our notation, we also define a horizontal Nusselt number as $\text{Nu}_\perp = q_\perp L / K \Delta T$. The symbol \perp indicates that the horizontal heat flux is perpendicular to the traditionally vertical heat flux (Nu) in Rayleigh-Bénard convection. Naturally, Nu_\perp is a dimensionless measure of the imposed horizontal flux and $S = \text{Nu}_\perp / \text{Nu}$ is the ratio between horizontal and vertical heat transfer rates. Another important number is the Reynolds number $\text{Re} = U_{\max} L / \nu = \text{Pr}^{-1} u_{\max}$, where the maximum velocity $u_{\max} = \max |\mathbf{u}|$ represents the flow speed scale. In order to investigate the strength of large-scale circulation, we also define the dimensionless total angular momentum as the integral $L(t) = \int_0^1 \int_0^1 [(x-0.5)v(x, y, t) - (y-0.5)u(x, y, t)] dx dy$, so a positive L represents counter-clockwise (CCW) large-scale circulation.

Overall, the system has three control parameters, or *inputs*: Ra , Pr and Nu_\perp . *Outputs* like Nu , Re , and L are functions of these inputs. To further simplify our study, we set $\text{Pr} = 4.4$ (water at 40°C) for all the simulations, as varying Pr in the range of 1 – 10 does not significantly change our results.

Denoting the vorticity as $\omega = \hat{\mathbf{k}} \cdot \nabla \times \mathbf{u}$ and the stream function as ψ such that $\mathbf{u} = \nabla_\perp \psi = (\psi_y, -\psi_x)$, we can write the Navier-Stokes equation in the vorticity-stream function format

$$\frac{\partial \theta}{\partial t} + \mathbf{u} \cdot \nabla \theta = \Delta \theta \quad \text{in } \Omega, \quad (2.1)$$

$$\frac{\partial \omega}{\partial t} + \mathbf{u} \cdot \nabla \omega = \text{Pr} \Delta \omega + \text{Pr} \text{Ra} \frac{\partial \theta}{\partial x} \quad \text{in } \Omega, \quad (2.2)$$

$$-\Delta \psi = \omega, \quad \mathbf{u} = \nabla_\perp \psi \quad \text{in } \Omega, \quad (2.3)$$

with boundary conditions

$$\left\{ \begin{array}{l} \psi = \psi_n = 0 \quad \text{on } \partial \Omega, \\ \theta = 0 \quad \text{on } \partial \Omega_{\text{up}}, \quad \theta = 1 \quad \text{on } \partial \Omega_{\text{down}}, \\ \frac{\partial \theta}{\partial n} = -\text{Nu}_\perp \quad \text{on } \partial \Omega_{\text{left}}, \quad \frac{\partial \theta}{\partial n} = \text{Nu}_\perp \quad \text{on } \partial \Omega_{\text{right}}. \end{array} \right. \quad (2.4)$$

To solve these equations, we employ a pseudo-spectral scheme (Peyret 2002) that uses the Chebyshev method. Spatial variables are discretized on the Chebyshev nodes, with operations like derivatives and integrations performed through corresponding discrete operators. Moreover, an efficient anti-aliasing filter (Hou & Li 2007) is applied when evaluating nonlinear advection terms pseudo-spectrally. At each timestep, a second-order implicit-explicit Adam-Bashforth Backward-Differentiation method solves for the stiff parabolic equations and the nonlinear equations. Typically, the simulation has 200 Chebyshev nodes in each dimension, and the timestep is

set as $\Delta t = 2 \times 10^{-4} \cdot \text{Ra}^{-1/2}$ [considering $|\mathbf{u}| \sim \text{Ra}^{1/2}$ (Ahlers *et al.* 2009)] to maintain numerical accuracy and stability.

3. Results

3.1. Flow and temperature profiles

The effect of adding a horizontal heat flux to Rayleigh-Bénard convection is directly reflected in the temperature and flow fields. Figure 2(a)-(d) show four time-averaged flow and temperature profiles at different magnitudes of horizontal flux. At a constant $\text{Ra} = 10^8$, the Nusselt number for the classical Rayleigh-Bénard convection ($\text{Nu}_\perp = 0$) is $\text{Nu}_0 \approx 25$, and the direction of circulation is not deterministic [Fig. 1(c) and Fig. 2(a)]. A clear influence of the horizontal flux is already present at $\text{Nu}_\perp = 4$ [Fig. 2(b)], where the direction of circulation becomes deterministically clockwise due to the buoyancy driven flows near the vertical walls. For $\text{Nu}_\perp \geq 16$ [Fig. 2(c)-(d)], the profiles of temperature and flow fields are dictated by the sidewall heating and cooling and the corner rolls are eliminated, similar to the profiles in a horizontal convection without bottom heating or top cooling (Belmonte *et al.* 1995). As a measure of relative strength between horizontal and vertical flux, $S = \text{Nu}_\perp / \text{Nu}$ is in the range of 0 - 1.5 in Fig. 2.

With increasing Nu_\perp , the Reynolds number stays at a similar level despite the increasing sidewall heating, which only seems to thin the vertical boundary layers near the sidewalls as shown in Fig. 2(b)-(d). Another consequence of this thinning of boundary layers can be seen in Fig. 2(i), where the time-averaged total angular momentum $|L|$ decreases with increasing Nu_\perp . This response seems to be counter-intuitive at first, but can be explained after examining the flow fields. As the magnitude of flow speed stays at a similar level, a thin boundary layer and a lack of bulk circulation [*inset* of Fig. 2(d)] lead to a reduced bulk contribution to the total angular momentum $|L|$.

The time-averaged temperature distributions along the horizontal center line $y = 0.5$ and the vertical center line $x = 0.5$ are shown in Fig. 2(e)-(f). On the horizontal cut $y = 0.5$, the temperature stays at $\theta(x, 0.5) = 0.5$ when no horizontal flux is added. As the sidewall heating-cooling increases, the temperature on the heating wall becomes higher while the temperature on the cooling wall becomes symmetrically lower. This change of temperature generates buoyancy jets along the two sidewalls, which can also be seen in Fig. 2(a)-(d). Due to flow advection, thermal boundary layer develops near the sidewalls as shown in Fig. 2(d), similar to the boundary layer profile near a heated or cooled vertical wall in an infinite space (Schlichting & Gersten 2016). As the buoyancy jets move upward/downward, they are diverted to the right/left as they meet the top/bottom wall, resulting in an overall clockwise circulation. Due to the relatively hot/cold fluid coming from the region near the left/right wall, the vertical temperature profile $\theta(0.5, y)$ in Fig. 2(f) has an inversion with a temperature rise near the top wall and a drop near the bottom. Namely, the bulk fluid becomes increasingly stratified. As a result, the magnitude of the temperature gradient near the top and bottom wall is increased, as shown in the inset of Fig. 2(f), leading to a higher vertical heat transfer rate.

Defining $\theta_l = \theta(0, 0.5)$, $\theta_r = \theta(1, 0.5)$, and $\theta_c = \theta(0.5, 0.5)$ to be, respectively, the temperature of the left wall, right wall, and bulk center, their time-averaged values at different Nu_\perp are shown in Fig. 2(g). The temperature rise and drop of the left and right wall are symmetric with respect to the bulk center, which has a mean temperature $\theta_c = 0.5$. Defining $\Delta\theta_\perp = \theta_l - \theta_c = \theta_c - \theta_r$ to be the temperature change on the sidewall, it increases with the horizontal flux Nu_\perp as shown in Fig. 2(h). Asymptotically, the measured data approaches $\Delta\theta_\perp \propto \text{Nu}_\perp^{4/5}$ when the side heating becomes dominant. This is consistent with the boundary layer scaling between the temperature rise ΔT_\perp and the injected heat Q from a vertical heated wall, $\Delta T_\perp \propto Q^{4/5}$ (Schlichting & Gersten 2016).

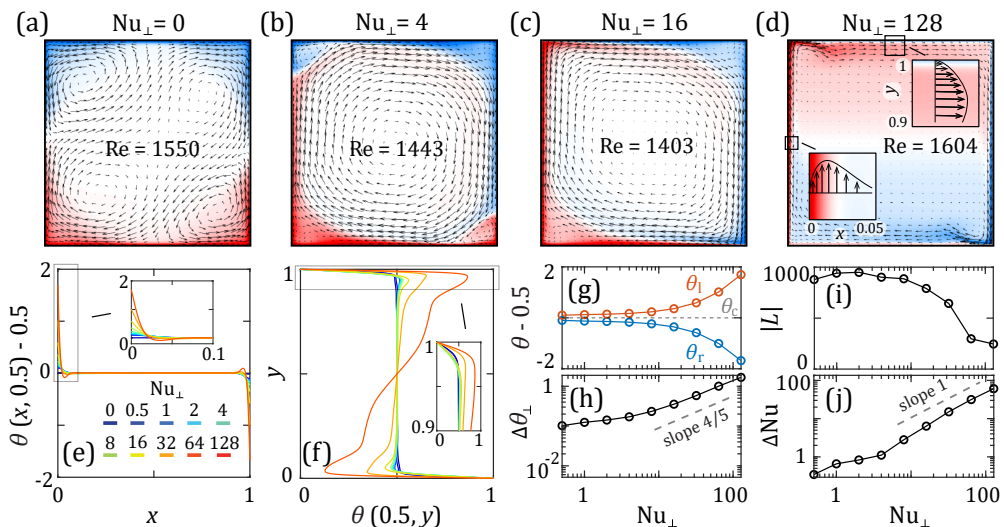


FIGURE 2. Flow (arrows) and temperature (color map) profiles of Rayleigh-Bénard convection with an additional horizontal heat flux. (a)-(d) Time averaged flow and temperature fields at $Ra = 10^8$ with four different strengths of horizontal flux. *Insets* of (d) show the boundary layer structure for the flow and temperature fields near the top center $(0.5, 1)$ and left center $(0, 0.5)$. Bottom and right boundary layers are symmetric to the top and left boundary layers with respect to the center $(0.5, 0.5)$. (e) Horizontal temperature profiles along $y = 0.5$. (f) Vertical temperature profiles along $x = 0.5$. (g) The time-averaged left wall temperature θ_l increases while the right wall temperature θ_r decreases symmetrically, about bulk θ_c , with increasing Nu_\perp . (h) At high Nu_\perp , the horizontal temperature change $\Delta\theta_\perp = \theta_l - \theta_c = \theta_c - \theta_r$ takes the $4/5$ power law as an asymptote. (i) Time-averaged total angular momentum $|L|$ decreases with the horizontal flux. (j) The Nusselt enhancement $\Delta Nu = Nu - Nu_0$ scales linearly with the horizontal flux.

Focusing on the enhancement of Nu , Figure 2(j) shows the Nusselt increment $\Delta Nu = Nu - Nu_0$ increases monotonically with Nu_\perp . Interestingly, the increment ΔNu scales linearly with Nu_\perp . An explanation for this is that the high and low temperature jets generated by the left and right sidewalls must pass by the top and bottom plates, leading to higher temperature gradients in the boundary layers shown in Fig. 2(f). Overall, the horizontal flux gradually limits the fluid circulation to a thin boundary layer region near four boundaries as shown in Fig. 2(d), and the heat conduction within the boundary layer strengthens the heat transfer rate (Nu) in the vertical direction. In the following section, we will systematically review such a Nusselt enhancement at different Ra .

3.2. Bulk heat transfer and flow properties

Without the horizontal flux ($Nu_\perp = 0$), Nu_0 is known to depend on the Rayleigh number in a nonlinear way: When the Rayleigh number is below a critical number [around 1708 (Koschmieder 1993)], the viscous force suppresses fluid motion and the fluid behaves like solid, hence $Nu_0 = 1$; Increasing the Rayleigh number well beyond critical, a power law relation emerges as $Nu_0 \propto Ra^{0.29}$ despite local deviations. The more detailed dependence between Nu and Ra is summarized in the theory of Grossmann & Lohse (Grossmann & Lohse 2000). In our simulation, this relation is recovered as the dark blue data of Fig. 3(a). As we shall determine later, the critical Rayleigh number in our numerical system is near $Ra_c = 2415$, slightly higher than the theoretical value 1708 for an infinitely wide convection cell (Koschmieder 1993), but consistent with experiments and simulations conducted in finite domain (Hébert *et al.* 2010).

The behavior near Ra_c changes with the addition of a horizontal flux: Figure 3(a) shows that the Nusselt number can be greater than 1 when $Ra < Ra_c$ and $Nu_\perp > 0$. The side heating and

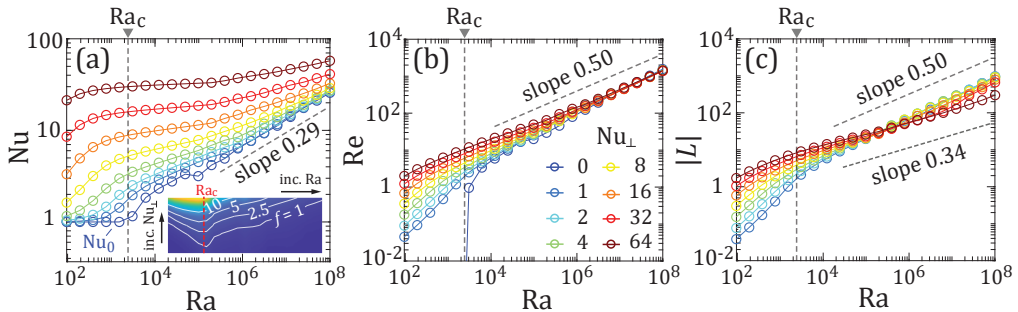


FIGURE 3. Time-averaged bulk quantities, Nu , Re , and $|L|$ measured at various Rayleigh number Ra and horizontal heat flux Nu_{\perp} . (a) The Nusselt number increases with Nu_{\perp} at a given Ra . The dark blue curve Nu_0 corresponds to the classic Rayleigh-Bénard convection with adiabatic sidewalls. *Inset*: Relative Nu enhancement $f = (Nu/Nu_0) - 1$ reaches a local maximum near $Ra_c = 2415$. Arrows indicate the direction of increasing Ra and Nu_{\perp} , where $Ra \in [10^2, 10^8]$ and $Nu_{\perp} \in [0, 64]$. (b) Horizontal flux leads to nonzero Reynolds number even for $Ra < Ra_c$, and $Re \sim Ra^{0.5}$ at high Ra is consistent with the scaling in classic Rayleigh-Bénard convection (Ahlers *et al.* 2009). (c) Total angular momentum $|L|$ has a 0.5 power law scaling with Ra when the horizontal flux is small, but takes a 0.34 power law when Nu_{\perp} dominates.

cooling set up the circulation even though the vertical temperature gradient is small, and this mixing effectively stirs the bulk fluid and increases the vertical flux. Indeed, Fig. 3(b)-(c) show that horizontal flux does lead to fluid motion with non-vanishing Re and L , even at $Ra < Ra_c$. Paying attention to the top half of the convection cell, the warm fluid close to the left wall flows upward to the top plate, creating a larger temperature difference between the fluid and the top plate and a smaller characteristic length as the boundary layer thickness decreases with the fluid velocity [Fig. 2(f)]. All together, these effects result in a greater temperature gradient near the top hence an enhanced Nu . Similar analysis can be performed symmetrically near the bottom plate, as the system is symmetric about its center such that $\theta(x, y) = 1 - \theta(1 - x, 1 - y)$.

This enhancement of Nu exists for a wide range of Ra and Nu_{\perp} . Shown in the *inset* of Fig. 3(a), the relative enhancement $f = (Nu/Nu_0) - 1$ is an increasing function of Nu_{\perp} when Ra is fixed. At a fixed Nu_{\perp} , however, the value of f peaks around the critical Rayleigh number Ra_c . One possible explanation for this peak is that the fluid (and hence the vertical heat flux) is easily perturbed when $Ra \sim Ra_c$ while the unperturbed Nu_0 is still at unity. As Ra increases, the relative enhancement f becomes smaller and approaches 0 asymptotically. This is understandable as the relative strength of the imposed horizontal flux and the unperturbed vertical flux Nu_{\perp}/Nu_0 diminishes with increasing Ra . Eventually, $Nu_0 \gg Nu_{\perp}$ as $Ra \rightarrow \infty$ so the horizontal flux has negligible effects on the Rayleigh-Bénard convection. In the same limit, the Reynolds number shown in Fig. 3(b) also returns to the asymptote of $Re \sim Ra^{0.5}$, consistent with the scaling in classic Rayleigh-Bénard convection (Ahlers *et al.* 2009) and suggesting the buoyancy flow generated by the top-bottom temperature difference determines the scale of flow speed.

The circulation of a perturbed Rayleigh-Bénard convection has a non-trivial dependence on Ra and Nu_{\perp} . Shown in Fig. 3(c), the time-averaged total angular momentum $|L|$ has a 0.50 power law scaling with Ra when Nu_{\perp} is fixed low, consistent with the scaling of $Re \sim Ra^{0.5}$, suggesting that the circulation rate is proportional to the flow speed. When Nu_{\perp} becomes higher, the scaling deviates and approaches an exponent of 0.34, perhaps due to the development of thin boundary layers near vertical walls seen in Fig. 2(b)-(d). This change of scaling for $|L|$ demands a more detailed analysis of the boundary layer structures, which awaits future investigations to justify. On the other hand, $|L|$ is an increasing function of Nu_{\perp} when holding a constant $Ra < 2 \times 10^5$, but this monotonicity is reversed for $Ra > 2 \times 10^5$ – increasing horizontal flux Nu instead leads to a decreased total angular momentum. It is known that the large-scale circulation

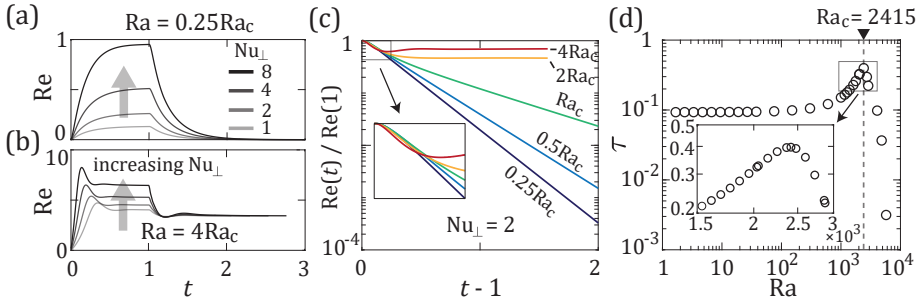


FIGURE 4. Perturbing Rayleigh-Bénard convection with a transient horizontal flux. An imposed horizontal flux during $t \in (0, 1)$ is removed after $t = 1$, allowing the system to relax back to the classical Rayleigh-Bénard configuration. (a) Reynolds number increases in below-onset Rayleigh-Bénard convection when a horizontal flux is added, and fluid motion diminishes after this flux is removed. (b) Reynolds number in the above-onset system decreases to the usual level of Rayleigh-Bénard convection after the perturbation is removed. (c) The fluid motion decays exponentially in the below-onset Rayleigh-Bénard convection after the perturbation is removed. (d) The relaxation time τ reaches a maximum at $Ra_c = 2415$, approaches a constant as $Ra \rightarrow 0$, and decreases rapidly when $Ra > Ra_c$. $Nu_{\perp} = 2$ in (c)-(d); cases with different values of Nu_{\perp} , shown in (a)-(b), yield similar τ at a fixed Ra .

only exists beyond a sufficiently large Ra (around 10^7), and very little circulation exists for low Ra convection. Therefore, the addition of horizontal flux to low- Ra convection generates an otherwise nonexistent circulation and hence increases the total flow angular momentum. At high Ra , increasing Nu_{\perp} does not change Re significantly [Fig. 3(b)] but the flow becomes confined in a boundary layer [Fig. 2(d)], so $|L|$ consequently reduces as the bulk's contribution to the angular momentum integral gradually diminishes.

3.3. Relaxation of a perturbed Rayleigh-Bénard convection

In the following examples, we temporally impose a horizontal heat flux during the time $t \in (0, 1)$, and then turn it off at $t = 1$ (corresponding to the diffusion time L^2/κ) so the system is allowed to return to the configuration of classical Rayleigh-Bénard convection. Figure 4(a) shows how the fluid responds to such perturbations. The Reynolds number for both the below-onset [$Ra < Ra_c$, Fig. 4(a)] and above-onset [$Ra > Ra_c$, Fig. 4(b)] states increases while the horizontal flux is applied. This is expected as there is a horizontal temperature difference in the fluid, which results in convective motion without threshold.

When the horizontal flux is turned off, the flow speed, represented by the Reynolds number $Re(t)$, relaxes to that of Rayleigh-Bénard convection: In Fig. 4(a), the flow velocity drops to 0 as the system is below onset; in Fig. 4(b), the flow velocity decreases to a constant $Re(\infty)$. To assess how fast the system relaxes to its equilibrium state, we define a relaxation time τ through $Re(1) - Re(\tau) = e^{-1}[Re(1) - Re(\infty)]$, whose dependence on Ra is shown in Fig. 4(d). The relaxation time τ behaves non-monotonically when Ra crosses a critical value, which can be identified as $Ra_c = 2415$ in Fig. 4(d). Near Ra_c , a peak of relaxation time τ appears, suggesting a critical slowing down (Hohenberg & Halperin 1977). This can also be seen in the *inset* of Fig. 4(c), where the $Ra = Ra_c$ curve (green) decays the slowest. It is worth noting that, at the same Ra_c , the Nusselt enhancement f also reaches a maximum when holding Nu_{\perp} constant [*inset* of Fig. 3(a)].

In the below-onset system, the relaxation of temperature and flow fields is closely associated with the dissipation of energy through the diffusion of heat and momentum. In the extreme case of $Ra \rightarrow 0$, the flow speed is almost 0 and Eq. (2.1) becomes the heat equation, $\partial\theta/\partial t = \Delta\theta$, whose solution decays exponentially in time. The relaxation time of this exponential decay is set by the initial condition of θ and geometry, therefore independent of Ra . As the flow field is only

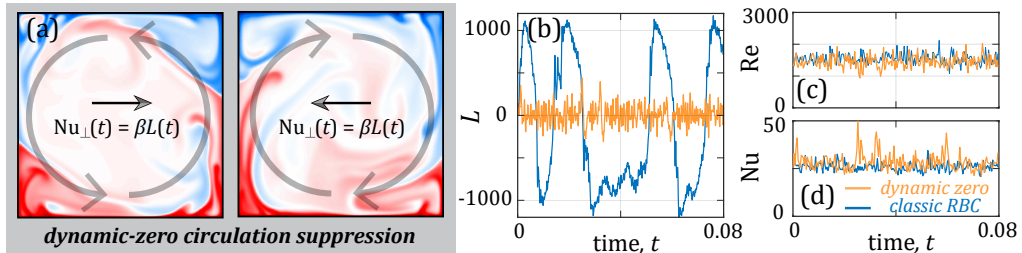


FIGURE 5. Actively controlling the Rayleigh-Bénard convection with a horizontal flux that depends on the strength of large-scale circulation, $Nu_{\perp} = \beta L$. (a) Two moments of the temperature fields and the dynamic-zero control. (b) The total angular momentum L stays close to 0 under the dynamic-zero control regime. (c) The Reynolds number of the controlled Rayleigh-Bénard convection is slightly reduced, while (d) the Nusselt number stays unchanged. Classic Rayleigh-Bénard convection (blue) data in (b)-(d) is the same as Fig. 1. Dynamic-zero regime in (a)-(d) has the same $Ra = 10^8$ and $Pr = 4.4$, and the control parameter is $\beta = 128$. Video of (a) is included in the Supplements.

driven by the temperature field, the magnitude of flow speed shall exhibit the same exponential decay in time. This confirms the exponential decay in Fig. 4(c), and explains why the relaxation time τ in Fig. 4(d) is almost constant for small Ra . Consequently, the dimensional relaxation time $T_{\tau} = L^2 \tau / \kappa \propto L^2 / \kappa$ has the same scaling as pure thermal diffusion in the limit of $Ra \rightarrow 0$.

Above Ra_c , the relaxation time in Fig. 4(d) decreases rapidly with Ra , as the vertical temperature gradient sustains fluid motion and the perturbation applied during $t \in (0, 1)$ is quickly “washed away”.

4. Discussion

In this work, we numerically explore the effects of an additional horizontal heat flux in Rayleigh-Bénard convection. We found that, in 8 decades of Ra , this horizontal heat flux induces fluid motion, modifies flow structures, and increases the Nusselt number. We observe a monotonic response in vertical heat flux when the horizontal heat flux is added, for convection both well-below ($Ra \sim 1$) and well-beyond ($Ra \sim 10^8$) onset, and this allows us to directly control the vertical heat transfer rate of Rayleigh-Bénard convection in a diverse range of parameters. By adding a horizontal flux, convection can also be initiated in an otherwise below-onset, conductive state. Once this flux is removed, fluid motion decays exponentially and the system returns to its equilibrium. Right at the critical Ra , the Rayleigh-Bénard system is most sensitive to the perturbation of the horizontal flux, where the highest Nu amplification ratio f and the longest relaxation time τ are reached. These nonlinear, non-monotonic behaviors of perturbed Rayleigh-Bénard convection could find future applications in the design of more complicated thermal devices.

As one example of achieving active control, we demonstrate a simple “dynamic-zero” mechanism to eliminate the large-scale circulation of Rayleigh-Bénard convection through adjusting the magnitude and direction of the horizontal flux. Shown in Fig. 5(a), we allow the strength of horizontal flux to depend on the total angular momentum such that $Nu_{\perp}(t) = \beta L(t)$, where β is a positive constant. With this control, a horizontal temperature gradient is induced so the resulting buoyancy torque counteracts the large-scale circulation. Two moments of such active control are shown in Fig. 5(a) and its video can be found in the Supplements. Indeed, Fig. 5(b) shows that the magnitude of total angular momentum L is suppressed through this dynamic-zero approach, and the Reynolds number is slightly decreased as shown in Fig. 5(c).

We would naturally ask, is the Nusselt number reduced without the large-scale circulation? It turns out that the Nusselt number in Fig. 5(d) stays unchanged, suggesting that the circulation

contribution is not significant. However, we have to point out that our dynamic-zero regime actively supplies horizontal flux to the Rayleigh-Bénard convection, which is known to increase its Nu. As we cannot isolate these factors, a more delicate approach is needed for future investigation of large-scale circulations. Nonetheless, active control is proven possible for the high Ra convection and it can successfully eliminate the otherwise persistent large-scale circulation. Among many avenues for harnessing Rayleigh-Bénard convection, the addition of horizontal flux is perhaps the simplest way of regulating one heat flux (Nu) with another (Nu_{\perp}), therefore serving a thermal purpose quite similar to the celebrated electronic transistor, and further bridging the thermal and electrical analogies.

REFERENCES

- AHLERS, G., GROSSMANN, S. & LOHSE, D. 2009 Heat transfer and large scale dynamics in turbulent Rayleigh-Bénard convection. *Rev. Mod. Phys.* **81** (2), 503.
- BAO, Y., CHEN, J., LIU, B.-F., SHE, Z.-S., ZHANG, J. & ZHOU, Q. 2015 Enhanced heat transport in partitioned thermal convection. *J. Fluid Mech.* **784**.
- BELMONTE, A., TILGNER, A. & LIBCHABER, A. 1994 Temperature and velocity boundary layers in turbulent convection. *Physical Review E* **50** (1), 269.
- BELMONTE, A., TILGNER, A. & LIBCHABER, A. 1995 Turbulence and internal waves in side-heated convection. *Phys. Rev. E* **51**, 5681–5687.
- BUSSE, F. 1978 Non-linear properties of thermal convection. *Reports on Progress in Physics* **41** (12), 1929.
- CHILDRESS, S. 2009 *An Introduction to Theoretical Fluid Mechanics. Courant lecture notes in mathematics*. Courant Institute of Mathematical Sciences.
- CHONG, K. L., YANG, Y., HUANG, S.-D., ZHONG, J.-Q., STEVENS, R. J. A. M., VERZICCO, R., LOHSE, D. & XIA, K.-Q. 2017 Confined Rayleigh-Bénard, rotating Rayleigh-Bénard, and double diffusive convection: A unifying view on turbulent transport enhancement through coherent structure manipulation. *Physical Review Letters* **119** (6), 064501.
- DU, Y.-B. & TONG, P. 1998 Enhanced heat transport in turbulent convection over a rough surface. *Phys. Rev. Lett.* **81**, 987–990.
- EVANS, L. C. 2010 *Partial Differential Equations. Graduate studies in mathematics*. American Mathematical Society.
- GROSSMANN, S. & LOHSE, D. 2000 Scaling in thermal convection: a unifying theory. *Journal of Fluid Mechanics* **407**, 27–56.
- GUO, S.-X., ZHOU, S.-Q., CEN, X.-R., QU, L., LU, Y.-Z., SUN, L. & SHANG, X.-D. 2015 The effect of cell tilting on turbulent thermal convection in a rectangular cell. *Journal of Fluid Mechanics* **762**, 273–287.
- HÉBERT, F. M. C., HUFSCHEID, R., SCHEEL, J. & AHLERS, G. 2010 Onset of Rayleigh-Bénard convection in cylindrical containers. *Phys. Rev. E* **81**, 046318.
- HOHENBERG, P. C. & HALPERIN, B. I. 1977 Theory of dynamic critical phenomena. *Rev. Mod. Phys.* **49**, 435–479.
- HOU, T. Y. & LI, R. 2007 Computing nearly singular solutions using pseudo-spectral methods. *Journal of Computational Physics* **226** (1), 379–397.
- HOWLE, L. E. 1997 Active control of Rayleigh-Bénard convection. *Physics of Fluids* **9** (7), 1861–1863.
- KOSCHMIEDER, E. L. 1993 *Bénard cells and Taylor vortices*. Cambridge University Press.
- NGUYEN, Q. M., ABOUEZZI, J. & RISTROPH, L. 2021a Early turbulence and pulsatile flows enhance diodicity of Tesla’s macrofluidic valve. *Nature Communications* **12** (1), 1–11.
- NGUYEN, Q. M., HUANG, D., ZAUDERER, E., ROMANELLI, G., MEYER, C. L. & RISTROPH, L. 2021b Tesla’s fluidic diode and the electronic-hydraulic analogy. *American Journal of Physics* **89** (4), 393–402.
- NIEMELA, J., SKRBEK, L., SREENIVASAN, K. & DONNELLY, R. 2000 Turbulent convection at very high Rayleigh numbers. *Nature* **404** (6780), 837–840.
- PEYRET, R. 2002 *Spectral Methods for Incompressible Viscous Flow. Applied Mathematical Sciences*. Springer New York.
- PURSGLOVE, S. D. 1960 Fluid “transistor” circuits. *Science and Mechanics Magazine* **06**, 81–83.
- SCHLICHTING, H. & GERSTEN, K. 2016 *Boundary-Layer Theory*. Springer Berlin Heidelberg.

- SCHMALZL, J., BREUER, M. & HANSEN, U. 2002 The influence of the Prandtl number on the style of vigorous thermal convection. *Geophysical & Astrophysical Fluid Dynamics* **96** (5), 381–403.
- SCHMALZL, J., BREUER, M. & HANSEN, U. 2004 On the validity of two-dimensional numerical approaches to time-dependent thermal convection. *EPL (Europhysics Letters)* **67** (3), 390.
- SCHÖNFELD, J. C. 1954 Analogy of hydraulic, mechanical, acoustic and electric systems. *Applied Scientific Research, Section A* **3** (1), 417–450.
- STEVENS, R. J. A. M., ZHONG, J.-Q., CLERCX, H. J. H., AHLERS, G. & LOHSE, D. 2009 Transitions between turbulent states in rotating Rayleigh-Bénard convection. *Phys. Rev. Lett.* **103**, 024503.
- WANG, Q., WAN, Z.-H., YAN, R. & SUN, D.-J. 2018 Multiple states and heat transfer in two-dimensional tilted convection with large aspect ratios. *Phys. Rev. Fluids* **3**, 113503.
- ZHANG, S., XIA, Z., ZHOU, Q. & CHEN, S. 2020 Controlling flow reversal in two-dimensional Rayleigh-Bénard convection. *Journal of Fluid Mechanics* **891**.
- ZHONG, J.-Q. & AHLERS, G. 2010 Heat transport and the large-scale circulation in rotating turbulent Rayleigh-Bénard convection. *J. Fluid Mech.* **665**, 300–333.